Loss enhanced transmission and collimation in anisotropic epsilon-near-zero metamaterials

Lei Sun, Simin Feng, and Xiaodong Yang

Related Articles

Understanding of nonlinear optical properties of CS2 from a microscopic viewpoint
J. Chem. Phys. 137, 084315 (2012)

Demonstration of nonlinear magnetoelectric coupling in metamaterials
Appl. Phys. Lett. 101, 051103 (2012)

Pure nonlinear optical activity in metamaterials
Appl. Phys. Lett. 101, 041911 (2012)

Light amplification in zero-index metamaterial with gain inserts
Appl. Phys. Lett. 101, 031907 (2012)

Taming the thermal emissivity of metals: A metamaterial approach
Appl. Phys. Lett. 100, 201109 (2012)

Additional information on Appl. Phys. Lett.

Journal Homepage: http://apl.aip.org/

Journal Information: http://apl.aip.org/about/about_the_journal

Top downloads: http://apl.aip.org/features/most_downloaded

Information for Authors: http://apl.aip.org/authors

Loss enhanced transmission and collimation in anisotropic epsilon-near-zero metamaterials

Lei Sun,[1] Simin Feng,[2] and Xiaodong Yang[1,a)]

[1]*Department of Mechanical and Aerospace Engineering, Missouri University of Science and Technology, Rolla, Missouri 65409, USA*
[2]*Physics Division, Naval Air Warfare Center, China Lake, California 93555, USA*

We verify the extraordinary transmission enhancement and collimation induced by the material loss in anisotropic epsilon-near-zero metamaterials, and reveal the physical mechanism of this exotic electromagnetic phenomenon via the iso-frequency contour analysis. In addition, we demonstrate the possibility in realization of such loss enhanced transmission of Gaussian beam in realistic silver-germanium multilayered structures by applying full-wave numerical simulations. © 2012 American Institute of Physics. [http://dx.doi.org/10.1063/1.4770374]

Recently, metamaterials with near-zero permittivity (epsilon-near-zero, ENZ) emerge into the focus of the extensive explorations in both theory and engineering due to their anomalous electromagnetic features at microwave and optical frequencies. ENZ metamaterials have been widely used in lots of exciting applications, such as directive emission,[1] electromagnetic energy squeezing and tunneling,[2–5] electromagnetic wave phase front shaping,[6,7] electromagnetic transparency,[8,9] and invisible cloaking.[10,11] In the previous work, it was shown theoretically that in ENZ media loss can induce transparency, omni-directional collimation, and transmission enhancement due to the interplay between ENZ and material loss.[12] Anisotropic loss can even improve the propagation of oblique incident beams.[12] In this letter, we verify such abnormal transmission enhancement in anisotropic ENZ metamaterials with full-wave numerical simulations together with the iso-frequency contour (IFC) analysis, and demonstrate the possibility in experimental realization of this phenomenon by using silver-germanium multilayered structures.

The propagation of a plane electromagnetic wave incident upon the flat interface (along the x-direction) between air and an anisotropic ENZ metamaterial is considered in two-dimensional space. The permittivity of air is set to be unity, and the principle components of the permittivity tensor for the anisotropic ENZ metamaterial are denoted as ε_x and ε_y, respectively. The permittivity ε_x is also set to be unity, i.e., $\varepsilon_x = 1$, while the permittivity ε_y reads $\varepsilon_y = \text{Re}(\varepsilon_y) + i\text{Im}(\varepsilon_y)$ with a near-zero real part $\text{Re}(\varepsilon_y)$ and a non-zero imaginary part $\text{Im}(\varepsilon_y)$ (the material loss). Regarding a plane electromagnetic wave in TM polarization (with non-zero field components E_x, E_y, and H_z), the dispersion relation of the anisotropic ENZ metamaterial reads

$$\frac{k_x^2}{\varepsilon_y} + \frac{k_y^2}{\varepsilon_x} = k_0^2, \tag{1}$$

in which k_0 is the wave vector in free space. The wave vector component k_x is real and determined by the incident wave, while k_y is complex and it is denoted as $k_y = \text{Re}(k_y)$

$+ i\text{Im}(k_y)$, with the imaginary part $\text{Im}(k_y)$ representing the propagation loss. The IFCs of the anisotropic ENZ metamaterial can be plotted based on the dispersion relation in Eq. (1). Figure 1 displays three different IFCs at the frequency of 193.4 THz (1.55 μm) corresponding to different values of permittivity ε_y, which has the same real part of $\text{Re}(\varepsilon_y) = 0.001$, but different material losses: the low loss $\text{Im}(\varepsilon_y) = 0.002$ (Fig. 1(a)), the moderate loss $\text{Im}(\varepsilon_y) = 2$ (Fig. 1(b)), and the high loss $\text{Im}(\varepsilon_y) = 20$ (Fig. 1(c)), respectively. The IFC of $k_x \sim \text{Re}(k_y)$ is plotted as red solid curve, while the IFC of $k_x \sim \text{Im}(k_y)$ is plotted as red dashed curve. The circular IFC of air with radius k_0 is also plotted as blue solid curve for comparison. Additionally, the incoming electromagnetic wave in air is represented by the wave vector $\boldsymbol{k}_{\text{in}}$ and the Poynting vector $\boldsymbol{S}_{\text{in}}$, while the electromagnetic wave inside the anisotropic ENZ metamaterial is represented by the wave vector $\boldsymbol{k}_{\text{ENZ}}$ and the Poynting vector $\boldsymbol{S}_{\text{ENZ}}$. As a particular example, $\boldsymbol{k}_{\text{in}}$ and $\boldsymbol{S}_{\text{in}}$ are marked as the incoming electromagnetic wave in air has an incident angle of 45°.

It is clear that for the low loss $\text{Im}(\varepsilon_y) = 0.002$ in Fig. 1(a), the IFC of $k_x \sim \text{Re}(k_y)$ forms a hyperbolic-like shape, with a very narrow opening toward the k_y-direction. Therefore, the direction of the transmitted power inside the ENZ varies from normal to nearly parallel to the interface. Moreover, the high propagating loss, represented by the IFC of $k_x \sim \text{Im}(k_y)$ prevents the electromagnetic wave from transmitting inside the anisotropic ENZ metamaterial even at small incident angles. Finite element method (FEM) full-wave simulations are used to illustrate the wave propagation behavior, where a TM polarized Gaussian beam is applied to mimic the experimental condition instead of the ideal plane electromagnetic wave. The Gaussian beam is represented by the distribution of the H_z component. Four different angles of incidence are calculated, including 15°, 30°, 30°, and 45°. The simulation results clearly indicate that for all these angle of incidence, the incoming Gaussian beam cannot couple into and transmit in the anisotropic ENZ metamaterial, but reflect back at the interface, which is consistent with the above IFC analysis. Thus, a low loss of the anisotropic ENZ metamaterial along the y-direction will prevent the transmission due to impedance mismatch. As the material loss is

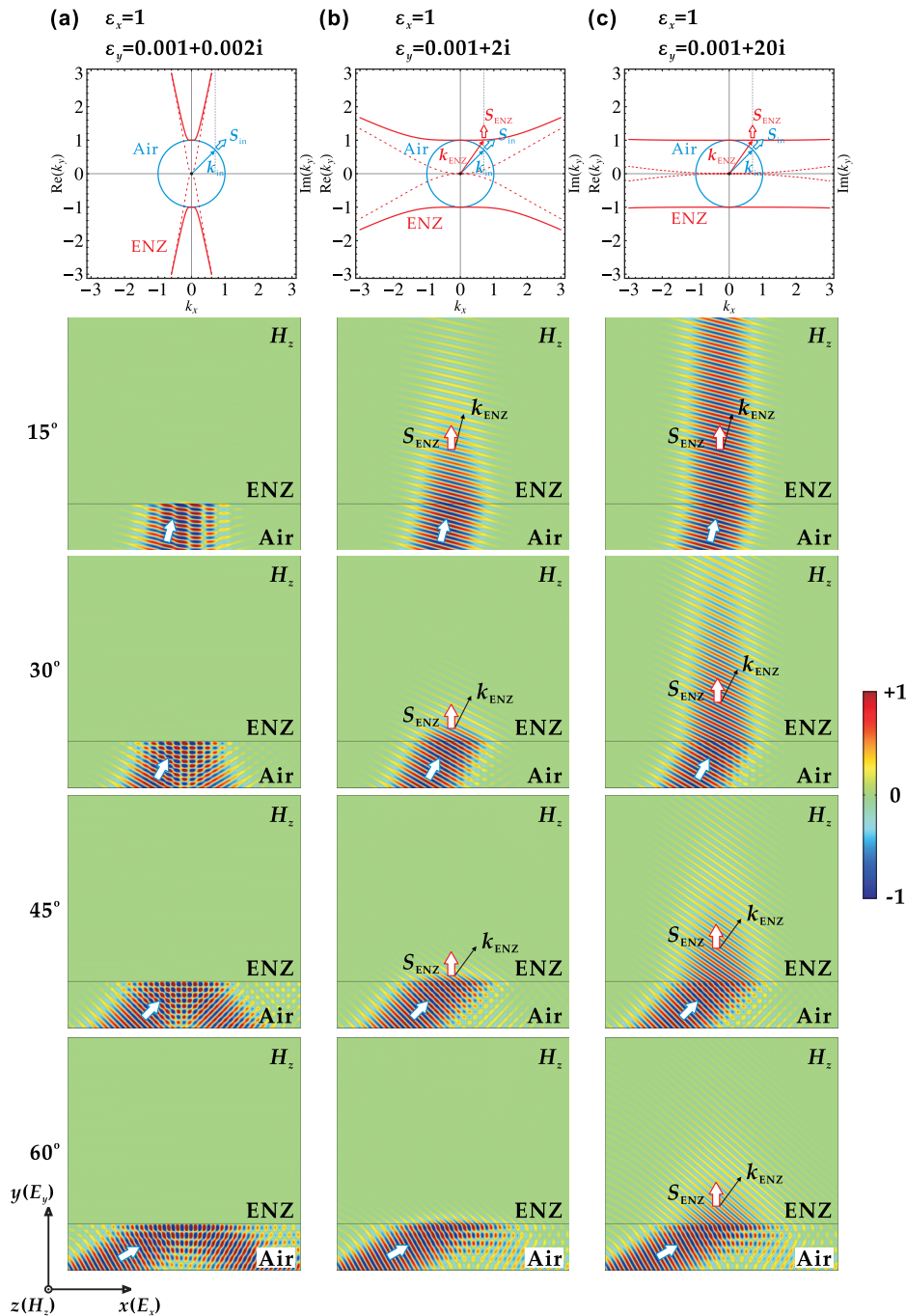a)Electronic mail: yangxia@mst.edu.

101, 241101-1

FIG. 1. The IFCs of the anisotropic ENZ metamaterial with different material losses, and the simulation results of the loss enhanced transmission in the anisotropic ENZ metamaterials. For the anisotropic ENZ metamaterial, the IFC of $k_x \sim \mathrm{Re}(k_y)$ is plotted as red solid curve, and the corresponding IFC of $k_x \sim \mathrm{Im}(k_y)$ is plotted as red dashed curve. The IFC of air is plotted as blue solid curve. The Gaussian beam is TM polarized and the distribution of the real part of H_z component is plotted. The incoming Gaussian beam is denoted by the wave vector $\boldsymbol{k}_{\mathrm{in}}$ and the Poynting vector $\boldsymbol{S}_{\mathrm{in}}$, with different angles of incidence, including 15°, 30°, 45°, and 60°. The propagating Gaussian beam inside the anisotropic ENZ metamaterial is denoted by the wave vector $\boldsymbol{k}_{\mathrm{ENZ}}$ and the Poynting vector $\boldsymbol{S}_{\mathrm{ENZ}}$.

increased to the moderate loss $\mathrm{Im}(\varepsilon_y) = 2$ in Fig. 1(b), the opening of the IFC of $k_x \sim \mathrm{Re}(k_y)$ toward the k_y-direction becomes wider, leading to a flatter curvature. Besides, the corresponding propagating loss for the oblique incidence also decreases due to the increased material loss.[12] Additionally, because of the flatter curvature of the IFC of $k_x \sim \mathrm{Re}(k_y)$, the incoming electromagnetic wave with small angle of incidence, e.g., less than 45°, will transmit inside the anisotropic ENZ metamaterial with the direction nearly normal to the interface, since the Poynting vector of the electromagnetic wave should be perpendicular to the IFC of $k_x \sim \mathrm{Re}(k_y)$. In the simulations, the Gaussian beam can transmit into the anisotropic ENZ metamaterial with a wide range of the angles of incidence from 15° to 60°. However, it is worth noting that the propagation distance of the Gaussian beam inside the anisotropic ENZ metamaterial is limited by its propagation loss, especially for the Gaussian beam with large angle of incidence, which is indicated in the IFC. Furthermore, the simulations also show that the wave propagation direction (indicated by the Poynting vector $\boldsymbol{S}_{\mathrm{ENZ}}$) of the Gaussian beam inside the anisotropic ENZ metamaterial is different from the direction of its phase velocity (indicated by the wave vector $\boldsymbol{k}_{\mathrm{ENZ}}$), due to the anisotropic permittivity profile. For the high loss $\mathrm{Im}(\varepsilon_y) = 20$ in Fig. 1(c), the IFC of $k_x \sim \mathrm{Re}(k_y)$ becomes almost flat straight lines, which allows the electromagnetic power inside the ENZ to propagate in the normal direction for a wide range of the incidence angle, for example, the Gaussian beam with 60° angle of incidence shown in the simulations. The relatively low propagation loss permits a long propagation distance of the transmitted electromagnetic wave inside the anisotropic ENZ metamaterial. As a consequence, the transmission is enabled and enhanced
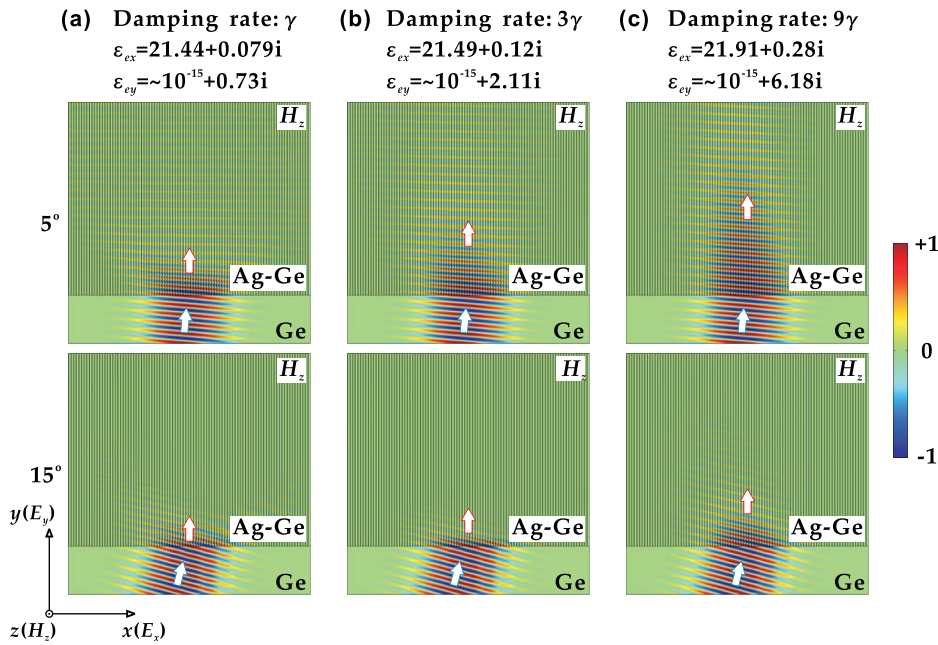
FIG. 2. The simulation results of the loss enhanced transmission in realistic silver-germanium multilayered stack, placed on a germanium substrate. The shaded area represents the multilayer stacking in the x-direction. The incoming Gaussian beam is TM polarized and the distribution of the real part of H_z component is shown at the ENZ frequency 193.4 THz (1.55 μm). The propagation direction of the Gaussian beam is denoted by hollowed arrows. Two different angles of incident, 5° and 15°, are considered with respect to three different damping rates, including γ, 3γ, and 9γ.

by the high loss of the anisotropic ENZ metamaterial along the y-direction.

Based on the effective medium theory,[13] we numerically demonstrate this exotic electromagnetic phenomenon with realistic metal-dielectric multilayered structures, as depicted in Fig. 2. The anisotropic ENZ metamaterial is constructed as a multilayer consisting of alternating thin layers of silver and germanium stacking in the x-direction. In order to reduce the reflection at the interface, the multilayered stack is placed on a germanium substrate. The thickness of each silver-germanium pair (along the x-direction) is 100 nm, and the effective permittivity of the stack can be represented as[13]

$$\varepsilon_{ex} = \left(f/\varepsilon_{Ag} + (1-f)/\varepsilon_{Ge} \right)^{-1},$$
$$\varepsilon_{ey} = f\varepsilon_{Ag} + (1-f)\varepsilon_{Ge}, \qquad (2)$$

where f is the filling ratio of the silver. The permittivity of the silver follows the simple Drude model $\varepsilon_{Ag} = \varepsilon_\infty + \omega_p^2/(\omega(\omega + i\alpha\gamma))$ with permittivity constant $\varepsilon_\infty = 5.0$, plasma frequency $\omega_p = 1.38 \times 10^{16}$ rad/s, and damping rate of bulk silver $\gamma = 5.07 \times 10^{13}$ rad/s. The additional factor α in the simple Drude model is used to account for the increased loss due to surface scattering, grain boundary effects in the thin silver film and inhomogeneous broadening in the realistic experiment.[14,15] In the simulation, three different values of factor α are considered, including $\alpha = 1$, $\alpha = 3$, and $\alpha = 9$, which results in three different damping rates: γ (Fig. 2(a)), 3γ (Fig. 2(b)), and 9γ (Fig. 2(c)). Moreover, the permittivity of germanium is $\varepsilon_{Ge} = 19.010 + 0.087i$,[16] and the ENZ frequency, at which $Re(\varepsilon_{ey}) = 0$, is designed at 193.4 THz (1.55 μm), thus based on Eq. (2) the filling ratio of the silver is $f = 0.129$ (Fig. 2(a)), $f = 0.130$ (Fig. 2(b)) and $f = 0.145$ (Fig. 2(c)), with respect to the different damping rates. A TM polarized Gaussian beam at the ENZ frequency 193.4 THz is considered in the simulation, and two angles of incidence, 5° and 15°, are calculated for each damping rate. Since lower damping rate leads to smaller material loss $Im(\varepsilon_{ey})$ along the y-direction in the

multilayered stack, it is clear that the Gaussian beam almost cannot couple into the silver-germanium multilayer stack and propagate inside for both angles of incident, although there is some optical scattering along the interface due to the layered structures. Furthermore, it is worth mentioning that the Gaussian beam splitting phenomenon shown in Fig. 2(a) inside the multilayered stack is caused by the optical nonlocality in ENZ metamaterials.[17,18] As the damping rate increases, as shown in Figs. 2(b) and 2(c), more energy of the Gaussian beam can enter into the stack for both angles of incidence, especially for the lower angle of incidence, resulting in a clear demonstration of the loss enhanced transmission in realistic metamaterial structures. Moreover, the simulation results also indicate that the Gaussian beam propagates inside the multilayered stack normal to the interface between the stack and germanium substrate, which agrees well with the above analysis.

To conclude, we have verified the extraordinary transmission enhancement and beam collimation caused by the material loss in anisotropic ENZ metamaterials through numerical simulations, and explained this phenomenon by applying the IFCs of anisotropic ENZ metamaterials. Furthermore, we also revealed the possibility in experimental realization of this phenomenon by using silver-germanium multilayered structures, which will stimulate experimental efforts to fabricate such anisotropic ENZ metamaterials and characterize this exotic optical phenomenon.

[1]S. Enoch, G. Tayeb, P. Sabouroux, N. Guérin, and P. Vincent, Phys. Rev. Lett. **89**, 213902 (2002).

[2]M. Silveirinha and N. Engheta, Phys. Rev. Lett. **97**, 157403 (2006).

[3]M. G. Silveirinha and N. Engheta, Phys. Rev. B **76**, 245109 (2007).

[4]R. Liu, Q. Cheng, T. Hand, J. J. Mock, T. J. Cui, S. A. Cummer, and D. R. Smith, Phys. Rev. Lett. **100**, 023903 (2008).

[5]B. Edwards, A. Alù, M. E. Young, M. Silveirinha, and N. Engheta, Phys. Rev. Lett. **100**, 033903 (2008).

[6]A. Alù, M. G. Silveirinha, A. Salandrino, and N. Engheta, Phys. Rev. B **75**, 155410 (2007).

[7]Q. Cheng, W. X. Jiang, and T. J. Cui, Phys. Rev. Lett. **108**, 213903 (2012).

[8]A. Alù and N. Engheta, Phys. Rev. E **72**, 016623 (2005).

[9]D. Rainwater, A. Kerkhoff, K. Melin, J. C. Soric, G. Moreno, and A. Alù, New J. Phys. **14**, 013054 (2012).

[10]J. B. Pendry, D. Schurig, and D. R. Smith, Science **312**, 1780 (2006).

[11]D. Schurig, J. J. Mock, B. J. Justice, S. A. Cummer, J. B. Pendry, A. F. Starr, and D. R. Smith, Science **314**, 977 (2006).

[12]S. Feng, Phys. Rev. Lett. **108**, 193904 (2012).

[13]D. J. Bergman and D. Stroud, Solid State Phys. **46**, 147 (1992).

[14]X. Yang, J. Yao, J. Rho, X. Yin, and X. Zhang, Nat. Photonics **6**, 450 (2012).

[15]Y. He, S. He, and X. Yang, Opt. Lett. **37**, 2907 (2012).

[16]S. Adachi, Phys. Rev. B **38**, 12966 (1988).

[17]R. J. Pollard, A. Murphy, W. R. Hendren, P. R. Evans, R. Atkinson, G. A. Wurtz, A. V. Zayats, and V. A. Podolskiy, Phys. Rev. Lett. **102**, 127405 (2009).

[18]A. A. Orlov, P. M. Voroshilov, P. A. Belov, and Y. S. Kivshar, Phys. Rev. B **84**, 045424 (2011).